J. A. Palenzuela · J. D. Jiménez-Perálvarez · R. El Hamdouni · P. Alameda-Hernández · J. Chacón · C. Irigaray

Integration of LiDAR data for the assessment of activity in diachronic landslides: a case study in the Betic Cordillera (Spain)

Abstract In the procedures to minimize diachronic landslides, data on their temporal evolution and destructive capacities are necessary. For that purpose, remote-detection techniques proved to be highly useful for quantifying the ongoing change in the relief, as well as in comparisons between digital terrain models achieved by Light Detection and Ranging. The methodology presented in this paper includes the supervised merging and comparison of sequential scans, acquired within nearly annual intervals from an irregular terrain, which improves the quality of the results highlighting ground changes. This approach is based on the processing of digital terrain models from point clouds acquired by Terrestrial Laser Scanning to quantify and interpret the landslide displacements. In parallel, it is supported by Global Navigation Satellite Systems, the use of artificial targets and a refined data processing to minimize the uncertainty and improve the precision of the results. This is applied to a large translational slide affecting phyllite rocks in a IV-V degree of weathering settled on the southern slope of Sierra Nevada (south-eastern Spain). During the monitoring period (2008–2010), the slide remained inactive until 2009, followed by a reactivation with displacements in the range −1.80 to 1.20 m along the period 2009–2010, where negative values are downwards from the reference model (2009). The accumulated relative standard deviation between data sets was on the order of 7.5 cm, whereas the threshold to determine a terrain displacement (also avoiding changes due to erosion-accumulation processes) was of 10 cm. When applying this methodology to Airborne Laser Scanning datasets for the years 2008 and 2010, covering zones hidden to the line of sight of the terrestrial technique, a reactivation with similar deformation pattern was found useful to validate the findings, although the detail of changes and quantitative results did not match exactly due to the different accuracy and resolution of both techniques. The reactivation of the slide coincided with a period of intense rains, pointing to this as the triggering factor, with a precipitation threshold of roughly 1000 mm in a period of 4 months, only reached on one occasion throughout in the historical record.

Keywords LiDAR · Laser scanner · Landslide activity · Ground movement · Betic Cordillera

Introduction

The socio-economic impact of landslides is high, being responsible for the loss of goods, services and sometimes human lives. The level of loss can be palliated when the problem is identified and recognized in space and time, given that landslides are among the most predictable and controllable natural phenomena, compared with other catastrophes such as earthquakes or volcanic eruptions (Brabb 1991). Nonetheless, gathering data and knowledge to predict the behaviour of this phenomenon is not easy. For instance, in the growing seasons or under the canopy, particularly small and shallow slope failures can be concealed, or they can be totally obliterated by agricultural practices, whilst well-aligned crops facilitate their recognition (Guzzetti et al. 2012). In addition, to assess the occurrence or temporal aspect of landsliding, other difficulties appear, like the lack of dedicated agencies with the responsibility to compile and update a landslide database. This matter can be overcome by preparing maps for fixed periods (e.g. annual frequency) on the basis of available imagery or, in general, remote sensing data (Van Westen et al. 2006).

One of the main measures for preventing and mitigating losses caused by slope-instability processes is the preparation of landslide inventory, susceptibility, hazard and risk maps (Brabb 1991; Guzzetti et al. 1999; AGS 2000; Chacón et al. 2006; Fell et al. 2008; Corominas et al. 2013). Many works have tried to evaluate the landslide hazard at the basin scale with the use of frequency analyses (Carrara 1983; Brabb 1984; Varnes 1984; Carrara et al. 1991, 1995; Soeters and Van Westen 1996; Chung and Frabbri 1999; Guzzetti et al. 1999; Chacón et al. 2006; Corominas and Moya 2008). However, the breadth of the spectrum of landslides makes it difficult to define a single methodology to evaluate their potential hazard (Chacón et al. 1996; Irigaray et al. 1996; Guzzetti 2002). Thus, the occurrence frequency and/or landslides evolution over a certain time period have traditionally been established by catalogues of historical movements (Chacón et al. 1993; Guzzetti et al. 2005).

The drawing of advanced landslide maps (hazard and risk) requires temporal data together with information on their destructive capacity. This is especially true in the case of diachronic movements, characterized by a time course that extends from minutes to dozens of centuries and that is expressed in different development stages and activity styles (Chacón et al. 2010). In these cases, a quantitative analysis of the diachronic evolution of the movement is necessary—that is, the degree of development and activity expressed in its geomorphological evolution (WP/WLI 1993, 1995; Cruden and Varnes 1996; Corominas and Moya 2008; Fell et al. 2008).

In this context, the use of techniques based on direct measurement data or aerial photographs to evaluate return periods has been applied to different works (Chandler and Brunsden 1995; Chacón et al. 1996, Flageollet 1996; Dikau and Schrott 1999; Gentili et al. 2002; Carrara et al. 2003; Casson et al. 2003; Walstra et al. 2004, 2007; Brückl et al. 2006). The use of precise data-acquisition techniques such as topographic instruments, GPS, laser scanner, photogrametry and remote sensing satellite systems represent a notable advance for tracking land movements. The joint use of these techniques enables an approximation of the hazard level in the context of landslides at the regional level (Jiménez-Perálvarez 2012); however, digital photogrametry and systems based on laser

are highly appropriate to study the temporal evolution of individual slope movements (Delacourt et al. 2007; Fernández et al. 2011; Irigaray and Palenzuela 2013).

The systems based on Light Detection and Ranging (LiDAR) adapted for the use of Terrestrial Laser Scanning (TLS) or Airborne Laser Scanning (ALS) provide a significant advance in the analysis of geomorphological changes in landforms due to landsliding phenomena (Baltsavias 1999; Glenn et al. 2006; Breien et al. 2008; Brideau et al. 2012). This distance scanning technique indeed allows the monitoring, characterizing and quantifying of changes in the relief (Teza et al. 2007; Abellán et al. 2010; Dunning et al. 2010). Depending on the flight time and an infrared pulse reflected over the slope surface, a high-resolution point cloud is recorded, corresponding to the terrain surface. With several sequential records on different dates, from the treatment and analysis of the data, the three-dimensional variation undergone by the morphological characteristics of the terrain over time is detected and quantified (Rosser et al. 2005; Oppikofer et al. 2009). In this way, it is possible to estimate the historical evolution of the landscape, regardless of the forest canopy, since the traces of the landslides can be tracked without difficulty (Carrara et al. 2003).

The first LiDAR applications in geomorphology date to the end of the 1990s (Baltsavias 1999) and have been perfected in the last decade (Delacourt et al. 2007). The different applications coincide in the capability to exploit high data of high redundancy, what enhances the topographical modelling of the scanned objectives and gives opportunities and flexibility to measure 3D deformations in the analysis phase through advancing tools (Monserrat and Crosetto 2008). In relation to landslides, this technique is applied, among other reasons, to detect deformations of a natural talus prior to the generation of rockfall (Abellán et al. 2010); to determine the quantity of displacement on natural slopes (Bitelli et al. 2004; Teza et al. 2007; Oppikofer et al. 2009); and to record the morphological and geometric characteristics of targets (Dunning et al. 2010). However, this technique is still difficult to handle computationally, as well as to edit the cloud of points resulting from the scan or, even, to apply the technique to large areas (González-Díez et al. 2014). By other side, to guarantee reliability and quality of 3D measurements through sequential LiDAR acquisitions, it is stated that the error increases with the distance to the analysed object, but also with common steps like the co-registration of multiple scans, which must to be considered in every approach in such a way of maximizing the coverage of the objective but minimizing systematic errors (Giussani and Scaioni 2004; Monserrat and Crosetto 2008).

This work presents a systematic methodology with three main aims: (1) to achieve the precision of the technique for quantifying surface deformation from data acquired from a long distance; (2) to assess its applicability to areas characterized by temporary, intermittent and irregular displacements; (3) to quantify the seasonal displacement that the landslide being studied underwent, in order to establish its activity and identify, if possible, the triggering factor. This is based on the time comparison in the same area of different digital terrain models (DTMs) formulated from the point clouds plotted using TLS and georeferences by global navigation satellite systems (GNSS). In addition, the work is supported by digital terrain models formulated by techniques based on ALS, useful as a complement, or for joint use, and validation of the models formulated by TLS. The methodology is applied to a translational slide on the southern slope of the Sierra Nevada, Granada (southern Spain).

Geological and geotechnical setting

The methodology was developed and refined for application and testing on a landslide of great dimensions (Almegíjar landslide). Its geomorphological features are clearly identifiable by laser scanning data processing. The slide lies on the bank of the Guadalfeo River, on the southern slope of Sierra Nevada (Granada, south-eastern Spain; Fig. 1). In this area, previous studies made by inventory maps and landslide-susceptibility maps, with information referring to the activity and degree of development (WP/WLI 1993, 1995; Chacón et al. 2006), manifest a considerable landslide incidence (Thornes and Alcántara-Ayala 1998; El Hamdouni et al. 2003; Fernández et al. 2003; Chacón et al. 2006; Irigaray et al. 2007; Jiménez-Perálvarez et al. 2011). These characteristics, together with surface erosion and human intervention, affect the socio-economic activities in the area when they interfere with the different elements at risk (numerous infrastructures and population centres) (Varnes 1984).

The slope morphology alternates between smooth and abrupt relief with over-excavated riverbeds, showing normal to wadi ("rambla" in Spanish) profiles and widespread landslides of variable size and typology. The dynamics of the slopes is linked to the performance of the wadi; thus, the landslides reactivation is related to flood periods, coinciding with periods of intense rainfall (Jiménez-Perálvarez et al. 2011). From the geological standpoint, the study area is within the Alpujarride Complex of the Internal Zones (Balanyá and García-Dueñas 1987) of the Betic Cordillera (Fig. 1). It is a metamorphic complex composed of different units marked by mechanical contacts with a sequence type composed, from below to above, of schists, quartzites, phillites, calcoschists and marbles (Gómez-Pugnaire et al. 2004). In the sector indicated, mainly phyllites and marbles of the Alpujarride Complex crop out together with post-tectonic Neogene and Quaternary materials, composed of silts, conglomerates, fluvial deposits and slope debris.

The Almegíjar landslide (36°54′5″N, 3°17′24″W; Fig. 1) is a translational slide in a developmental stage. It has an average height and slope of approximately 640 m and 35°, respectively. It affects primarily heavily weathered phyllites with levels of calcoschists. Its main scarp is almost vertical, towards ~130° while several secondary scarps, subparallel to the main one, constitute the source area of superficial debris slides.

With the aim of gather relevant information about the geotechnical characteristics of the materials affected by the landslide, seven Dynamic Probing Super Heavy (DPSH) and three test pits (TP) (Fig. 2a) together with Standard Penetration Test (SPT) testing and unaltered sampling were carried out during the field research.

Lithologically, the area is composed of grey phyllites with interbedded layers of calcoschists. The materials are heavily weathered (weathering grade IV-V; ISRM 1978) weak-jointed rock, showing discontinuities with a maximum opening of 1 cm and an average spacing of 10 cm. The laboratory samples were taken in the same family of discontinuities corresponding to the main shear plane. The fill of the discontinuities is made up of colluvial material from weathering of the phyllites and corresponds to low-plasticity clays and silts (CL-ML). It has an average plasticity index
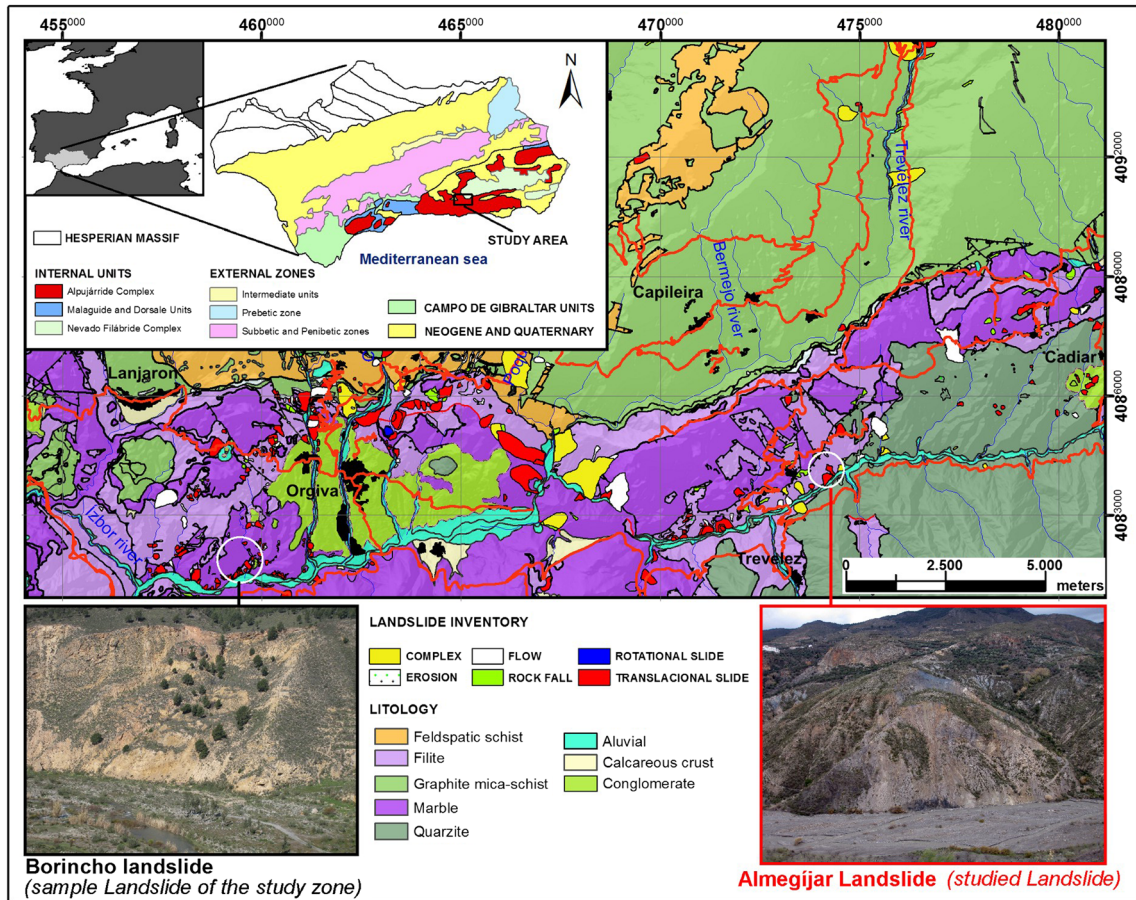
Fig. 1 Geographical and geological setting of the study zone

PI of 6 (liquid limit $W_L \approx 26$−plastic limit $W_P \approx 20$) and a Dispersion Index of ≈ 90 %. Therefore, this material is also highly susceptible to erosion. The areas with the least degree of weathering even preserve their original structure, with characteristics similar to the overconsolidated soils (with Over Consolidated Ratio OCR ≈ 1.5 and permeability $K \approx 10^{-4}$ m/s, according to the laboratory tests). The areas with the greatest weathering correspond to residual soils.

The correlation of corrected SPT blow values with the internal friction angle (ø) (Schmertmann 1975; Mayne et al. 2001) reached values within the range of 25° to 30°, which are correspondent to the residual values in phyllites (minimum values) and weathered
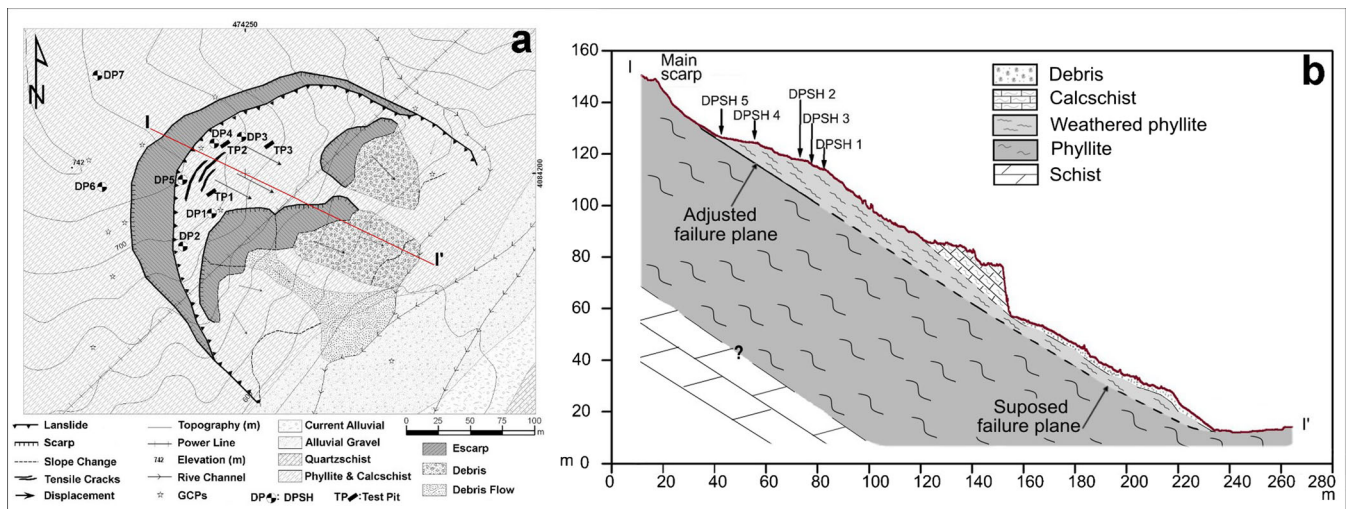

Fig. 2 The Almegíjar slide; **a** geomorphological scheme showing the position of the in situ tests; **b** geological cross section and interpretation of the shear plane

micaschists and phyllites (maximum values; Hunt 2005). These values are of the same order of magnitude as those derived through triaxial and ring shear tests in the case of residual strength ($\phi \approx 25°$ and cohesion $c \approx 5$ kPa). This material is consistent with the R_1 rock-type (very weak or highly weathered rock), attributed with a very low resistance to the uniaxial compression (1–5 MPa; Brown 1981). The Geological Strength Index (GSI) of the material, easily friable, can be established at values around 20, indicative of low to very low quality.

The DPSH blow values rises with depth, showing an increasing strength, but this trend is interrupted, according to the location of each test, between 7 and 11 m, where the number of blows decreases (reaching almost null values at 8.30 at DPSH-3). At depths greater than 11 m, again the resistance of the material generally increases. This pattern was not recorded outside the limits of the landside (stable area), where the general trend to increasing strength with depth was not interrupted (DPSHs 6 and 7). The results suggest the presence of a less resistant level of phyllites over the stable substrate of more competent phyllites. The two levels are separated by a layer of very low strength, which is interpreted as a shear plane (Fig. 2b) with mean slope of 30° in the direction N130E (in the area near the main scarp). The direction and inclination of the slide plane coincide with the orientation of the main set of discontinuities (30/130). In addition, the average slope of the whole supposed failure-plane (30°) approximates to the internal friction angle estimated for the body of mobilized rock.

The stability of the mobilized rock mass was defined according to the geomechanical characteristics, the geometry of the slide plane and the slope morphology, based on the generalized Hoek-Brown failure criterion for rock masses (Hoek and Brown 1980, 1997) and using the following conservative values: unit weight of the solid particles $\gamma_s = 23$ kN/m³; GSI=20 (blocky to disturbed structure with very poor surface conditions); uniaxial compression strength $\sigma_{ci} = 1.0$ MPa; constant of intact rock formed by phyllites $m_i = 7$; and disturbance factor=1 (without disturbances caused by blasting or mechanical excavation). In this way results a safety factor of SF=1.1, indicating a stage very close to the limit of equilibrium, making possible new reactivations in response to any triggering factor (rain, seismic activity, anthropogenic activities, etc.).

Methods and materials

The TLS or terrestrial LiDAR is based on the same principle as airborne LiDAR (ALS), except in this case the scanning is made from equipment stationary on the ground. Thus, this technique is known as ground-based LiDAR technology (Lichti et al. 2002). The most common case is that the levelled equipment is placed at a fixed point, which substantially simplifies the sensor as an inertial system is unnecessary. The needed instrumentation is the scanner itself and the equipment to record the absolute coordinates, generally a differential global positioning system (DGPS), although this could be dispensed when working with relative coordinates.

TLS instruments have high precision and are capable of working in different settings and under adverse atmospheric conditions. They use tachymetry measurements consisting of combinations of measurements of distances, angles and intensity of illuminated points. The basic practical principle consists of scanning the entire field of view (FoV) by the projection of an optical signal onto a given target, and the corresponding processing of the reflected signal in order to determine the distance between the target and its reflection. The result is a cloud of 3D points that represents the model scanned with centimetre resolution.

The monitoring of landslides by TLS requires long-range instruments (at least 500–1000 m) which provide at least centimetre accuracy. This is an ideal technique for slope cuts and steep slopes, although it can be used for slopes with low inclination, even at the cost of making a greater number of scans (Irigaray and Palenzuela 2013; Palenzuela et al. 2013). The main limitations are the extent of the area to scan and the hidden parts of the areas with very low slopes or in the direction opposite to the beam, which would require a higher number of scans to avoid "shadow" areas. In the processing, the difficulties are the same as with airborne LiDAR—that is, the relative orientation between scans and the filtering of the elements that do not belong to the terrain in the strict sense (Glenn et al. 2006; Sterzai et al. 2010). Therefore, in the procedure of 3D scanning, multiple scans are usually made from different positions to reduce the shadows. Each of these point clouds will be contained in a coordinate system for each position, and afterwards a fusion is made of all of them. The complete process, from the data acquisition to the viewing of the graphic information, is what is known as the "3D pipeline" (Bernardini and Rushmeier 2002).

In the present study, the system used was TLS Riegl® (Modelo LMS-Z420i; Laser Measurement System 420i; Riegl 2010), composed of a distance explorer of the type Time of Flight (ToF), which provides points measurements on position and distance in spherical and Cartesian points (Teza et al. 2007). This technology provides a high density of measurements (thousands of points per second) with centimetre accuracy and repeatability. The scanned data were processed and analysed with the specific software RiscanPro® (Riegl 2010).

The uncertainty of the positioning measurement, in a plane perpendicular to the direction of the laser beam, was determined by the distance to the observation target and the angle divergence of the beam (Lichti and Jamtsho 2006, Riegl 2010), which reaches 0.25 mrad/50 m in the used measuring instrument. In addition, the linear uncertainty in the distance measured to the target reaches 1 cm plus the proportion of 20 ppm of the resulting distance. On the slope studied, with observation distances of less than 600 m, the uncertainties in the measurement distance were below 22 mm, whilst the uncertainty by the laser footprint (as consequence of its angle divergence) was below 125 mm perpendicular to that distance.

In addition to the distance measurements, the conventional technique of positioning and orientation by means of a target set up away from the scanner or Back-Sighting Point (BS), also referred as direct georeferencing (Scaioni 2005), was applied to the present work. Thereafter, the cylindrical target acting as the BS was finely scanned together with the point cloud from one scan position and its centre was extracted using the scan software. During the landslide scanning (~35 min), dual frequency observations were gathered using the rapid-static method with post-processing by means of two GNSS (GPS + GLONASS) receptors: one mounted on the scanner (see Fig. 4b) to calculate its origin geodetic coordinates, while the second one remained measuring on the vertical line of the cylindrical target centre (see Fig. 4c). The differential correction of the position obtained through the observations was

performed by using the offsets measured in situ and the Receiver Independent Exchange (RINEX) file from the closest Andalusian Positioning Network (R.A.P) permanent reference station together with its geodetic coordinates. Lastly, these two points allowed orientating the scan in the global coordinate system. In this way, the position with the highest precision for the global positioning led to a standard deviation of 11 mm for the horizontal component and 17 mm for the vertical one.

The changes in the landforms—that is, the comparison of terrain models corresponding to different dates—were quantified and interpreted based on the general work flow to process TLS data. Nonetheless, particular attention has been devoted in critical steps, improving the quality of the global point cloud to generate every DTM, as well as applying adequate methods in the comparison of consecutive DTMs and the supervised zonation focused in the revealing of landslide activity changes. Thus, the applied methodology can be summarized in the following stages (Fig. 3 and Table 1).

Planning and data recording

This stage includes the programing of the sequential acquisition of data (Table 2) and positioning of the scanning base stations, in such a way that the complete target area is covered in order to construct the DTM minimizing shadows areas but also the cumulative uncertainty due to the alignment of several point clouds [(1) in Fig. 3, and Fig. 4d]. Regarding the different alternatives to address the scans alignment, artificial targets were installed both

Fig. 3 Flow chart of the methodology used

in the inner and outer parts of the landslide [(2) in Fig. 3, and Fig. 4a], which facilitates the rapid fusion of data sets. The targets situated in the inner parts were used to align the data recorded on the same date, while the outer ones (stable zones) were used to correlate sequential point clouds. Although these targets were only set up in order to streamline the point cloud registration, this step was proved to be solved even in the absence of them, so they were no used as permanent scatters. Accordingly, this methodology neither involves the measurement of the target's geodetic coordinates in such inaccessible areas; rather, the global positioning is performed through the direct georeferencing. So that, only a target was placed functioning like an artificial BS point, visible in a straight line from the scanner position.

Once the planning is defined, the TLS and GNSS receivers (Fig. 4b, c) are placed in the positions previously established, scanning data from positions (PA in Fig. 4d) between 500 and 600 m away from the landslide area [(3) in Fig. 3]. In the scanning positions, the geodetic coordinates of the scanner's own coordinate system (SOCSi) and the corresponding BS were recorded by two GNSS-calibrated receptors (Fig. 4c), later corrected in post-process and used to carry out the direct georeferencing of the SOCSi and BS in the global coordinate system (GLCS).

Data processing

This is the most important stage of the methodology, whose quality will affect the reliability of the final results allowing their correct interpretation. Accordingly, as above mentioned, special attention was put on processes like data adjustment and filtering, comparison of sequential DTMs and zonation of differential displacements.

Point cloud reduction

The dispersion of each point cloud (resulting from the fusion of the scans for a date) was minimized by applying an Octal Tree structure (OCTREE) filter, whilst optimizing the processing of the data at software and hardware levels [(4) in Fig. 3]. To keep the representativeness of the original scanned surface, the filter output consists of centres of gravity coming from cubes of 0.1 m side, close to the mean point cloud resolution.

Georeferencing of the global coordinate system

Avoiding induced misalignment by consecutive orientation of several point clouds, only the system of the scanner position (SOCSi) with the highest precision for the global positioning (as stated previously, 11 mm for the horizontal component and 17 mm for the vertical one) was selected as project coordinate system (PRCS) and georeferenced into the GLCS, beginning from the BS and SOCSi-corrected coordinates [(5) in Fig. 3].

Alignment

Once the data are acquired and the PRCS established, each set of point clouds for a date has to be merged in one global point cloud by solving their roto-translation matrixes. This process can be done via manual assignment of connecting points [(6) in Fig. 3] between each point cloud and the fixed one (PRCS), or faster through the automatic pairing of common targets (fine or automatic registration) if at least three targets were set up on the ground and then were scanned [(7) in Fig. 3].
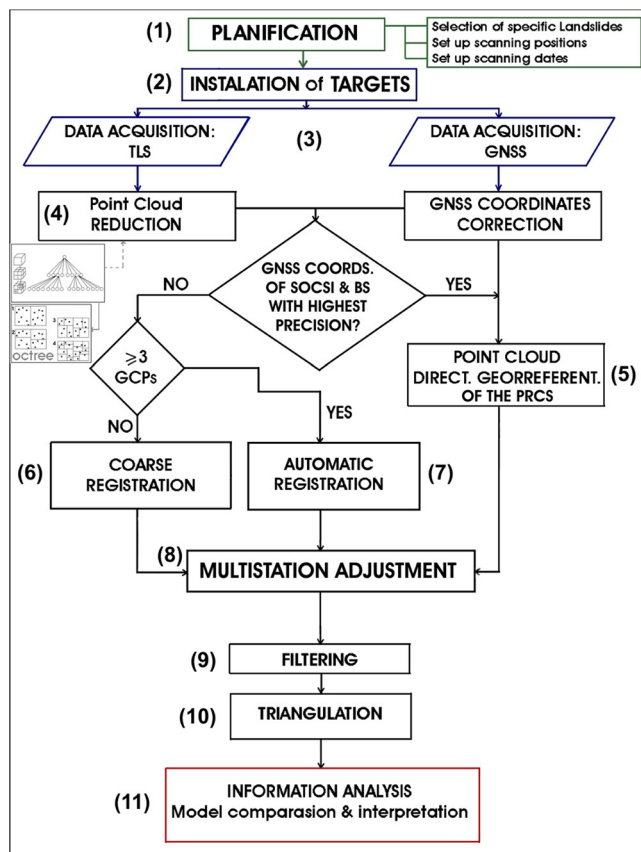
Table 1 Stages followed in the applied methodology

Stage	Task	Observations
Acquisition planning	Selection of scanning points	Location of the minimum number of positions for optimal analysis. Minimize holes, interferences, occlusion of satellite signals, shadows, etc.
	Scanner timing	GPS and GLONASS almanacs, confirmation of the dilution of precision (DOP)
Field work	Placement of targets	Optional, access to the area of interest may be unfeasible or risky
	Acquisition of TLS and GNSS data	Installation of TLS and GNSS receptors (calibrated on the scanner and BS point). Record ≥30 min (fast static). Successive: monthly to annually
Desk work	Data processing	Reduction of the point clouds, correction of the GNSS coordinates, alignment, multi-station adjustment, filtering, triangulation
	Analysis of the compiled information	Application of algorithms and methods for calculating distances, supervised classification, determination of land forms

In the Almegíjar landslide, aligned by fine registration, the standard deviation of the aligned data sets ranged between 1 and 7.7 cm.

Multistation adjustment

To improve the merging of the point clouds aligned by the previous process, they were subsequently adjusted to the reference point cloud [(8) in Fig. 3] by using the multistation adjustment (MSA). The procedure is based on the iterative closest point (ICP; Besl and McKay 1992; Teza et al. 2007). Once a point cloud is fixed as a reference dataset, every run of the ICP algorithm tries to overlap the other point clouds onto the reference one. This is basically done by applying iteratively rototranslation to subsets from those point clouds, until they are relocated as close as possible to their corresponding points into the reference dataset. To tackle with this task, before every run, the ICP needs the input of the distance or radius R, which constrains the spherical space of the distance between the points of every pair of connecting points (tie-points) which are iteratively located during the automatic matching of the problem dataset and the reference dataset. Beside R, a convergence limit for the SD has to be set, representing the minimum error to stop de run. Generally, R is reduced before every run of the adjustment, as the point clouds of the common object are increasingly overlapping and the residual SD decreases. However, by the experience, when checking the number of corresponding points in the statistics results, as well as their spatial distribution after every run, it can be observed how SD decreases, but also the number of corresponding points does. Consequently, it can be observed that the distribution of corresponding points is constrained to some parts of the merged point cloud when SD values are too low, indicating that these parts are better adjusted than other. So the process has to be supervised in order to get a good adjustment but ensuring a homogeneous merging throughout the entire object (scanned terrain in this case); otherwise, smaller SD could result in a poor merging. This adjustment resulted in a final standard deviation between 0.5 and 2.5 cm in the Almegíjar landslide. Thus, finally the errors involved by this methodology are summarized as three different errors. The first one is the standard deviation from the absolute positioning adjustment, showing a horizontal uncertainty of 11 mm, unlike the vertical one which attains 17 mm. The second error is related to the uncertainty of the point position when measuring through the scanner range finder in the own coordinate system, with the ellipse of higher uncertainty consisting of axes with 22 and 125 mm long, as explained before. Lastly, the third error is related to the relative uncertainty resulting from the cumulative standard deviations

Table 2 LiDAR-based technique and corresponding date by point of acquisition in the sequential scanning of the Almegíjar landslide

Technique	Point of TLS acquisition (Fig. 4c)	No. of scans	Date
TLS	PA1	1	15/07/2008
	PA2	1	15/07/2008
	PA3	1	15/07/2008
ALS	Strip	1	11/08/2008
TLS	PA1	1	10/03/2009
	PA2	1	10/03/2009
	PA3	1	10/03/2009
ALS	Strip	1	18/05/2010
TLS	PA1	1	11/06/2010
	PA2	1	11/06/2010
	PA3	1	11/06/2010

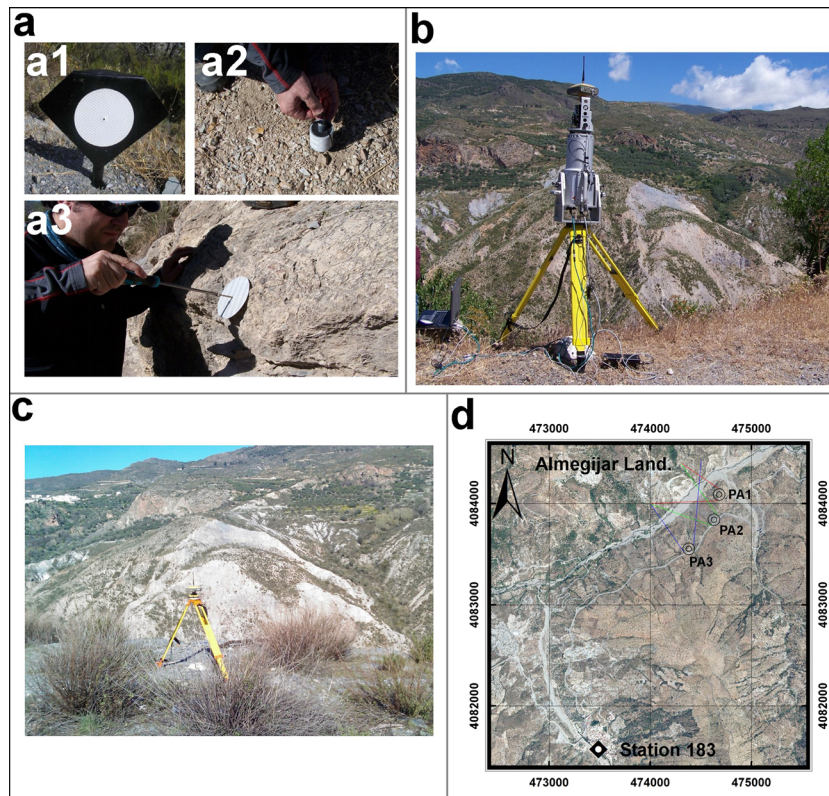*TLS* Terrestrial Laser Scanning, *ALS* Airborne Laser Scanning

Fig. 4 **a** Targets of flat type situated within (*a3*) and outside (*a1*) the landslide and cylindrical target (*a2*); **b** TLS Riegl® equipment working in the PA3 position; **c** GNSS receptor registering the SOCSi position of the PA2 analysis point; **d** location of the Almegíjar landslide and Station No. 183 (*PA* = points of TLS acquisition)

obtained from the MSA, composed by three adjustments performed (three scanned data set superimposed to the reference or fixed one), once the global point cloud of the project is fixed. Thus, considering the mean standard deviation (1.5 cm) for each run of the MSA, the total standard deviation will result in 4.5 cm, while the maximum will reach values lower than 7.5 cm in either direction (3D uncertainty).

Filteringm of the unacceptable features by the specific analysis
Elements such as trees, shrubs and/or vegetation in general represent a noise when comparing sequential digital elevation models (DEMs). Therefore, to keep only the ground changes, after finishing the adjustment stage, this noise is filtered out [(9) in Fig. 3]. Totally automatic filtering by different approaches (progresive segmentation, statistics or minimum values on a base mesh, etc.) present multiple uncertainties in irregular terrain, as in the present study case, due to misclassification of the elements between terrain and other classes. Therefore, this stage is carried out by a semi-automatic method consisting of the elimination of the floating points that become uncoupled at their positions as sets of outliers on the general dispersion of the global cloud of points. This consists of the selection and subsequent displacement of adjacent sections throughout the point cloud with variable wide (generally from 2 to 20 m), depending on the density of the observed vegetation and/or on the irregularity of the terrain.

Triangulation
After the filtering stage, a mathematical reference model is constructed to compare temporal data, creating a triangular irregular network (TIN) using the Delaunay triangulation algorithm (Boris 1934) [(10) in Fig. 3].

Information analysis: model comparison and interpretation of the results

The final aim is to compare the previous and subsequent positions of the surveyed surfaces, applying an adequate method to reveal and interpret landslide differential displacements [(11) in Fig. 3]. This procedure consists of calculating the minimum-distance vectors, after the adjustment, between the reference model and another data set (mesh or point cloud). That is the minimum distance between the source point cloud (which models the surface for the later date) and the reference one (which models the surface for the previous date). This procedure becomes more viable the more regular the study object and the more rigid the slope deformation. However, the shapes of the landslides topography do not usually correspond to the surfaces where the curvature gradient follows approximately constant trends, where this technique is more reliable. For this reason, the algorithm of the normal vectors implemented in the scanner software and illustrated in Fig. 5 was applied in the present work. Once the surfaces are in their adjusted positions, the minimum distance (D_i) is calculated from the points or nodes (q_i) of the source point cloud to the point, p_i, belonging to the average plane representing the closest part on the reference mesh in the orthogonal direction to this plane (Fig. 5b).

When dealing with this task, a reference plane parallel to main planes (XY, XZ, YZ) could be chosen, or any other created
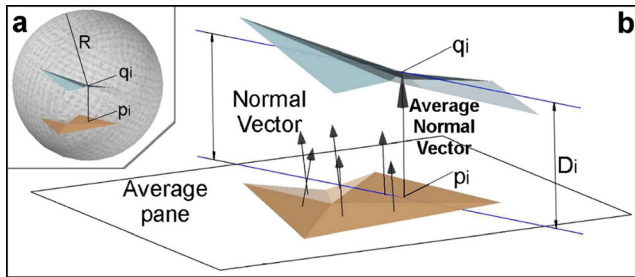
Fig. 5 **a** Search-radius R from point p_i at the closest reference surface to the point q_i at the problem surface; **b** determination of the distance D_i

by the user in the orientation that is believed to be the most appropriate for every inferred displacement. However, to overcome the difficulty of define multiple reference planes on large natural surfaces in the correct orientations perpendicular to the main displacements, the Euclidean distances D_i were calculated providing conservative distances close to the minimum component, given in the normal direction from the original surface. Therefore, the distance (D_i) is calculated from q_i to a reference surface determined by the average plane (Fig. 5b) of those polygons placed within the closest area within the reference DTM (that of the previous date). Equally than in the case of the adjustment process, to find those polygons, a radius of search is specified, with origin in q_i and a length (R) as to include the highest displacements (Fig. 5a). The average normal vector (Fig. 5b) corresponding to that surface, crossing q_i, will intersect the reference surface at p_i, determining D_i as the distance between both q_i and p_i.

The main constraint of this method is that the relative parallel displacements between two planar surfaces are not detected unless the continuity is interrupted by a break on the scanned terrain. For instance, this is a typical effect in very low or creeping movements where the displacement is closest to the smooth slope, and the vertical changes can be so small that can be erroneously ignored. On the contrary, in the present study, the irregular morphology of the translational landslide shows a steep slope together with several break lines (Fig. 2); so, it deforms easier in directions not parallel to the ground surface, making possible to detect those displacement.

Once the displacements are calculated, the triangles adjacent to q_i are classified according to their values, giving as a result a distribution of the minimum displacement undergone in a direction approximately perpendicular to the reference surface or orientation of the average plane. This classification is made in a supervised way to detect slope features related to the landslide activity, which is performed by constraining the range of the classified displacements (with positive, negative or both types of limits) with expert criterion until the interesting terrain changes are highlighted. In this case, important changes were detected when the range of neutral zone from −10 cm to +10 cm was established. Since the total relative uncertainty is 7.5 cm, 10 cm has been considered as reasonable threshold because this interval involves both, the relative uncertainty and lower erosion-accumulation rates (see Figs. 6 and 7). The values were differentiated between positive when the last source point data or mesh is above the reference surface and negative when the contrary occurs.
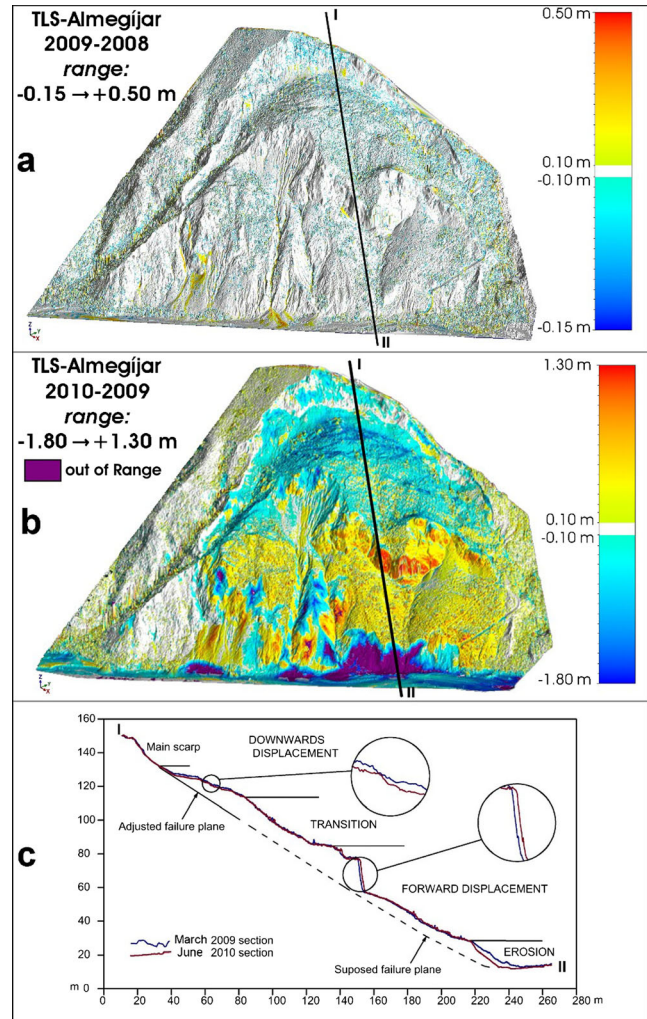

Fig. 6 Temporal displacement of the Almegíjar landslide. In *yellow to red* appear the positive values (accumulation of material); in *blue tones* the negative values (erosion or subsidence); in *purple* the unclassified interval; **a** period 2008–2009; **b** period 2009–2010; **c** topographical cross section showing the surface changes between March 2009 and June 2010

The negative values (−) were interpreted as areas of loss of relief by erosion, sinking, recession of the scarp, etc. The areas classified with positive values (+) correspond to sedimentation areas, advance of the slope mass, accumulation of slope debris, etc. Figure 3 shows schematically a flow diagram of the methodology used. Table 1 synthesises the different stages of the methodology, extensively developed in this section.

Results and discussion: geomorphological evolution of the Almegíjar landslide

As commented above (Table 2), three scanning sequences were executed on the following dates (Irigaray and Palenzuela 2013), and thereby, two landslide development intervals were assessed:

– 15 July 2008
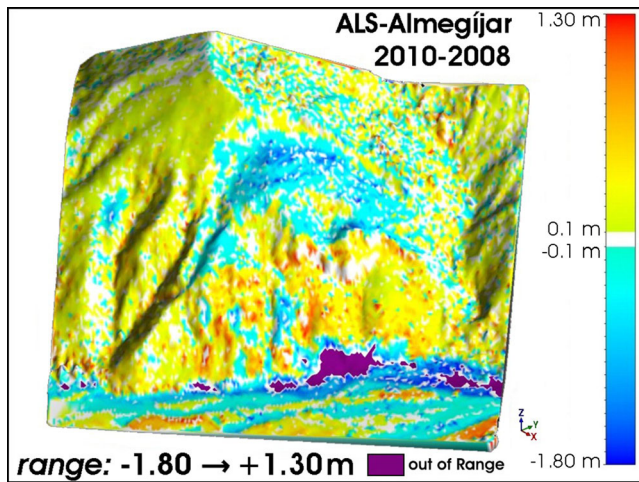– 10 March 2009
– 11 June 2010

Fig. 7 Temporal displacement of the Almegíjar landslide. Image classified for the data analysis of ALS of the period 2008–2010. The colour scale shows the variation in the displacements from a subsidence (in *blue tones*) in the upper part to an advance in the lower half of the mobilized mass (*yellow to red*). In *purple,* the unclassified range

Development interval 15 July 2008 to 10 March 2009

As aforementioned, the range of classification was established on a supervised way during the comparison between the DEMs for the years 2008 and 2009, selecting a suitable range to make easily distinguishable the ground changes. Thus, the terrain surface modelled for 2009 shows topographical variations with values ranging between −0.15 m and 0.50 m, with regards to the surface modelled in July 2008. For values between −0.10 m and 0.10 m, a neutral zone was established (white, not classified), filtering the existing noise (changes in vegetation and equipment uncertainty).

According to the slope morphology, such small variations can be attributed to erosive surface processes: denudation when scars appear on steepest parts as the major escarpment (blue tones on the top middle part of Fig. 6a), and deposit where an increasing volume can be observed forming a cone geometry on a flatter area (e.g. yellow to orange tones on the bottom middle part of Fig. 6a) or filling concave gullies. Naturally, the greatest erosion is concentrated in the high part of the scarp, while at the foot of the slides the thickness increases locally, corresponding to the cone-dejection deposits, where the maximum accumulation value is registered. These values are considered characteristic of geomorphological shift in the relief due to erosion. Therefore, deformational components of mass displacement are not observed and thus it can be concluded that in this time interval the landslide remained inactive for the detection precision of this methodology.

Development interval 10 March 2009 to 11 June 2010

In this case, during the supervised classification of the measured displacements, greater changes were detected, expanding the range between −1.80 and 1.30 m (with a neutral interval between −0.10 and 0.10 m). In this interval, the topographical variations observed between the two studied sequences in the period 2009–2010 were more relevant for the interpretation of the changes in the activity of the landslide. The deep incision

at the foot of the landslide presents values lower than −1.80 m (exceeding the classification range); this incision is due to the fluvial erosion of the riverbed and has not been classified (drawing in purple). Within the chosen range (classified), there is a clearly appreciable general advance of the lower half of the mass up to 1.3 m. In the upper part of the mass, the maximum orthogonal displacements between surfaces indicate an average subsidence of 0.70 m, with a maximum value of 1.20 m.

Deformation pattern from the processing of the data gathered by ALS (2008–2010)

Within the framework of the regional project P06-RNM-02125, two dataset of airborne LiDAR corresponding to 08/2008 and 05/2010 were acquired. These LiDAR data sets provided the opportunity to be processed in order to compare the results with those obtained from the analysis of TLS data. The major difference between the ALS equipment and the static TLS lies in the fact that in the first, the trajectory of the SOCS is given by the Inertial Navigation System (INS) and Differential Global Positioning System (DGPS). Despite the aid of these systems to solve orientation and positioning, some misalignment errors between two consecutive models can appear, and therefore the adjustment is also necessary. Due to the characteristics of the ALS, the greater distance from the equipment to the ground (≈2000 m for both acquisitions) and the speed of the aircraft, the results from ALS processing are inherently less precise than those derived from the TLS processing. In this research, a Leica ALS50-II was used, with an error in distance below 0.30 m, and its footprint illuminates an area of 0.32 m². By adjusting the two databases, the standard deviation of the residues improved from 0.870 to 0.173 m, as resulted from previous research carried out at the study area (Palenzuela et al. 2014). The resolution of ALS is also lower that in the TLS survey. The mean point-density for the data of the first acquisition resulted in 0.31 points/m², while for the second one resulted in the very similar figure of 0.34 points/m² (Palenzuela et al. 2014). This is supposedly an ALS disadvantage as compared with the TLS; however, there are holes or zones that cannot be scanned from the TLS positions but only from the line of sight of the ALS and vice versa. In this context taking advantage of the availability of both data sets, the resulting models were obtained and compared. Despite the data were acquired from these different techniques, the deformation pattern obtained by comparing their results are very similar, although the different resolutions and accuracies make difficult to converge in the same quantitative results. Referring to the processing of ALS data, the results (Fig. 7) show a maximum advance in the mobilized mass (at the middle of the height of the slide), above 1.25 m, and a subsidence in the upper part greater than 1 m.

Triggering factors

The main factors triggering landslides are earthquakes and high precipitation (Wieczoreck 1996; Guzzetti et al. 2005). The lower threshold of magnitude for which an earthquake can generate landslides could be estimated at 4.0, although, to cause considerable instability, large earthquakes are necessary (M_w >6.0; Rodríguez-Peces et al. 2009). The seismic record of the study area, between 1924 and 2004, presents more than 1000

earthquakes with a mean depth of 12.5 km, where only 20 earthquakes present a magnitude greater than 4.0 and none higher than 5.0. On the other hand, in the study zone, no direct association is found between earthquakes and currently observable slides (Jiménez-Perálvarez 2012). Therefore, in the study area, the expected earthquakes, following the Spanish Seismic Hazard Map, are not considered a probable source of triggered landslides (at least not by the expected major ones), and the slope instability in the study area is related to other phenomena. Slides are also often generated after a period of days or months of intense rains (Guzzetti et al. 2005; Irigaray et al. 2000). In the study area, diachronic landslides are common, showing a long and "intermittent" development by alternating quiescence and activity periods until the depletion stage (Chacón et al. 2010). In this area, the periods of greater quantities of accumulated rainfall appear as the main consequence of mass movements. Deeper landslides are initiated or reactivated by long-term and intensity rainfall (Zhang et al. 2006; Crosta and Frattini 2008). In this case, landslides are indirectly initiated, reactivated or accelerated when the rainfall infiltrates throughout the deepest layers and the enough pore-water pressure is reached decreasing the shear strength (Iverson 2000). Furthermore, other processes as the increasing in the water level of adjacent channels and the toe undermining, as it is shown in purple in Figs. 6b and 7 (erosion out of range), can affect the landslides stability.

In this sense, the existing rainfall record (from 1945 to 2012) was reviewed from the station (Stat. No. 183 Torvizcón) near the landslide site (Fig. 4d). The analyses made indicate that the mean annual precipitation for the Almegíjar sector (Stat. No. 183) is 554.4 mm. The highest monthly values are reached in the month of December, with values of 95.2 mm. For the monitoring period by TLS (2008–2010), a maximum value was found during the month of December 2009 (377 mm). This value represents almost 400 % of the monthly average for the rainiest month in the study area (Table 3).

In the Almegíjar sector (Fig. 8), the cumulative rainfall for the period 2008–2009 exceeds the average, but no month represents
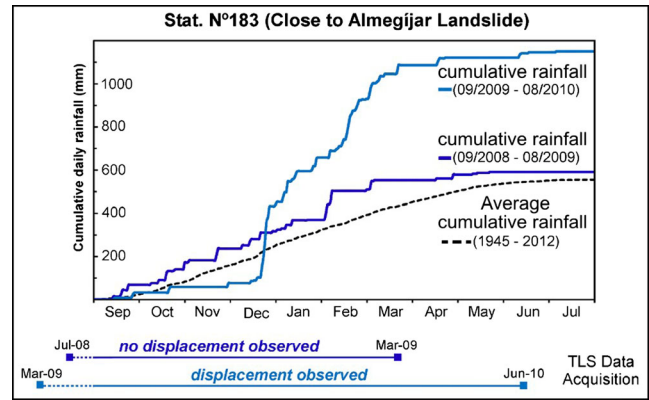

Fig. 8 Cumulative rainfall for the periods 2008–2009 (*dark blue*) and 2009–2010 (*light blue*), and average accumulated daily precipitation at the end of the year (*broken black line*). The TLS acquisition dates are indicated, as well as whether displacement or slides were detected

more than 215 % of that average (212.6 % in February 2009, approximately double the average (Table 3)). Considering the rainiest interval (from December to March), the cumulative rainfall for 2008–2009 represents only 107.7 % of the average cumulative rainfall for 1945–2012. These values have not been sufficient to reactivate the slide during this period. However, for the period 2009–2010 (Fig. 8), the precipitation of December 2009 to March 2010 is far above the average, reaching values of 1010.5 mm. These values represent more than threefold the average in the rainiest months (Table 3).

The results of the analysis by TLS indicate the reactivation of the landslide during this period of intense rains, which exceeds the average by threefold. This supports the idea that the reactivation of the landslide is the consequence of the intense precipitation registered between December 2009 and March 2010, what supposed a new historical record within rainfall series available for 66 hydrologic years (Fig. 9) and which acts as a triggering factor.

Table 3 Cumulative rainfall by month and for the periods October–March and December–March, considering the values corresponding to hydrological years 2008–2009 and 2009–2010 and the mean for the interval 1945–2012 at Torvizcón (station no. 183), near the Almegíjar landslide

| Station	Record	Precipitation (mm)							
		Oct.	Nov.	Dec.	Jan.	Feb.	Mar.	Oct.– Mar.	Dec.– Mar.
Stat. no. 183-Torvizcón. Sector Almegíjar	Mean1945–2012	59.1	75.0	95.2	72.0	64.9	61.4	427.6	293.5
	Year 2008–2009	104.4	65.1	87.0	47.9	138.0	43.3	485.7	316.2
	% with respect to the mean	176.6 %	86.8 %	91.4 %	66.5 %	212.6 %	70.5 %	113.6 %	107.7 %
	Year 2009–2010	27.0	17.5	377.0	205.0	273.5	155.0	1055.0	1010.5
	% with respect to the mean	45.7 %	23.3 %	396.0 %	284.7 %	421.4 %	252.4 %	246.7 %	344.3 %
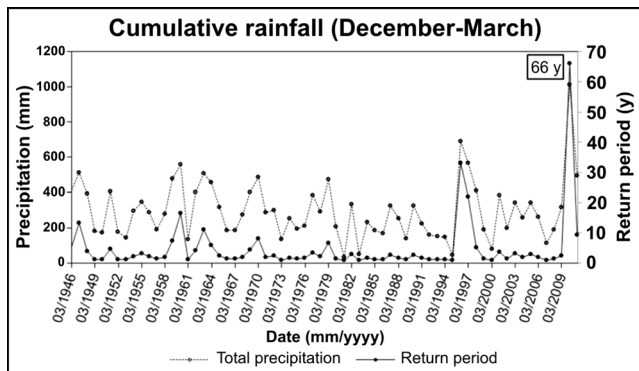
Fig. 9 Cumulative rainfall for the interval December to March (1945–2011) showing an historical record in the hydrologic year 2010–2011

Conclusions

In the procedures to minimize the risk of diachronic landslides, data are needed on the evolution and destructive capacity of landslides. Remote detection-based techniques, such as the comparison of the terrain models generated from TLS data, are of great utility, though some peculiarities (i.e. supervised adjustment and classification) have to be taken into account to get good results. The basis of this approach is as simple as comparing DTMs of different dates and classifying the changes in a supervised way. To reach this phase, previous steps addressed to refine the final digital models (minimizing hidden areas, orientation of point clouds, adjustment, filtering, etc.) are streamlined by following the present methodology, enabling successive analyses of data acquired sequentially. By other hand, nowadays, LiDAR technology and the interface of its handling software have experienced such improvements as to be used in an easy way, although with the necessary knowledge and skills. In addition, as was done during the development of the present research, the survey equipment can be rented or the service of acquisition hired. In some countries, some official organizations provide open data produced by different sensors (including LiDAR (x, y, z) files and orthophotograph). For example, in the study area, regional data can be found in the "Service for Download Orthophotographs and data from the territory" (REDIAM 2014) or in the National Geographic Institute (IGN 2008–2012). The availability of these services and products make the costs increasingly similar to those of other topographical techniques (Total Station or DGPS surveys), however, getting a much more detailed survey in short time. The accuracy of the results depends on factors such as the equipment used or the distance to the target. Support from global positioning techniques (GNSS), the placement of the targets and/or the processing techniques themselves minimize the uncertainty and make the results more accurate. Also, the contrast of the results with those from another source (e.g. ALS) enables the validation and comparison of the results.

The methodology developed in this research offers the following results:

The differential displacements calculated and classified in the Almegíjar landslide show that from July 2008 to March 2009, only erosion and superficial deposit characteristic of the natural geomorphological evolution of the relief occurred; therefore, in this period, the mass movement remained inactive. However, between March 2009 and June 2010, reactivation occurred, developing a deformation that shortened the length of its longitudinal axis with a perpendicular extent, giving place to an arched form of the mobilized mass. This fact is in agreement with the metastable state of equilibrium (SF≈1) determined for the very poor quality rock mass (GSI≈20) characterized from the geotechnical parameters, as well as confirms the sequential activity of a diachronic and deep landslide, which has been reactivated after a dormant stage. Within this reactivation phase, the maximum displacements could be established around 1 m, that considering the period between data acquisitions involves a maximum time span or minimum movement rate and, consequently, minimum intensity. This rate only could be significant if elements at risk were located immediately on the mobilized mass or within the landslide run out distance (advancing displacements). The movement resulting from the analysis of the point clouds acquired by means of ALS between November 2008 and May 2010 are equivalent in orientation to those already registered by TLS; however, and as expected from the lesser accuracy and resolution, the magnitude and level of detail are not totally equivalent to those of the TLS.

In this research using TLS technology (coupled with GNSS), small variations in the geomorphological characteristics of the landsliding area were detected. In a translational slide of large dimensions, generated on highly weathered phyllites and beginning from distances between 500 and 600 m from the target (slope) to the measurement point (equipment), the method begins to be effective when the movements recorded are greater than the accumulated SD of 7.5 cm (cumulative uncertainty). In any case, the displacements found are greater than the total relative uncertainty of the method, which, together with the similar results regarding the deformation patterns found by processing ALS data, may be considered meaningful for the assessment of the landslide activity. The findings indicate a landslide reactivation within a specific time interval (2009–2010) and regarding this LiDAR-based methodology. Nonetheless, the total uncertainty can conceal minor (or slower) displacements which can be revealed by using other techniques (e.g. DiNSAR), providing that their requirements are fulfilled (e.g. maximum displacements determined by the radar wavelength, $\lambda/2$, in the Line of Sigth in the case of DiNSAR), and no other factors are concealing landslide displacements or producing important noise (e.g. loss of congruence in the measurement of phase differences in the case of DiNSAR).

On the other hand, no displacements were detected in less rainy period (e.g. 2008–2009), whereas the reactivation of the Almegíjar landslide coincides with a period of intense rains between December of 2009 and March 2010, what supposed a new historical record within rainfall series available for 66 hydrologic years. This reflects that the precipitation in this latter period (1010 mm) was related to the triggering of this last event of landslide displacements. Hence, it could be established that, in the recorded landsliding event, the slide reactivates when the cumulative precipitation reaches values of roughly 350 % of the local average cumulative precipitation during a period equal to or less than 4 months, which corresponds to a rainfall of about 1000 mm. Thus, the Almegíjar landslide was reactivated as consequence of the accumulated rainfall during enough time as to infiltrate throughout the deepest layers, while the water flow what rose throughout the adjacent channel produced the toe undermining. These indirect phenomena related to the long wet period ended in

a new landslide destabilization. Nonetheless, this is only a preliminary critical threshold, until further researches, based on the continuity of monitoring together with the recording of climate and hydrologic parameters (i.e. integrated monitoring), could extent its validity for a wider period. While nearly annual monitoring by using the TLS technique was shown effective to display small deformation changes, the increasing in the frequency of data acquisitions would provide better information to enable a suitable interpretation on the development of subsequent reactivations. In this way, the rainfall threshold could be better approached, as well as the partial influence of one or more causes (toe undermining, pore-pressure increasing as consequence of the infiltration or water level at the toe) resulting from the cumulative rainfall could be determined.

In conclusion, the methodology developed provides information on the evolution or expected change of the activity in diachronic slides related to the recurrence of triggering events. It detects differences in topography that can predict the sudden slope failure without the need to access the unstable zone. The applied laser-scanning technique gives the density of direct measurements (3D point cloud) with high resolution (decimetre) and enables the discrimination of the smallest features detected in over the target area, in comparison to other techniques (<10 points/m^2 in ALS; ~5 m in DInSAR). Nevertheless, the more information covering wider periods, and gathered throughout future application of the present methodology, together with the measurement of in situ climate and hydrologic parameters, the more accurate and meaningful the critical level of rainfall linked to the reactivation of the landslide. Consequently, larger datasets generated for a longer term could provide useful information in quantitative hazard and risk assessment; in the case of diachronic landslides, by quantifying the differential displacements within established time periods.

References

Abellán A, Calvet J, Vilaplana JM, Blanchard J (2010) Detection and spatial prediction of rockfalls by means of terrestrial laser scanner monitoring. Geomorphology 119:162–171

AGS (2000) Landslide risk management concepts and guidelines. Australian Geomechanics Society, Sub-committee on landslide risk management, 44pp

Balanyá JC, García-Dueñas V (1987) Les directions structurales dans le Domaine d'Alborán de part et d'autre du Détroit de Gibraltar. Comptes Rendus de l'Académie des Sciences de Paris. Comptes Rendus de l'Académie des Sciences de Paris Serie II 304(15):929–932

Baltsavias EP (1999) Airborne laser scanning: basic relations and formulas. ISPRS Int Soc Photograme 54:199–214

Bernardini F, Rushmeier HE (2002) The 3D model acquisition pipeline. Comput Graphics Forum 21(2):149–172

Besl PJ, McKay N (1992) A method for registration of 3D shapes. IEEE Trans Pattern Anal Mach Intell 14(2):239–256

Bitelli G, Dubbini M, Zanutta A (2004) Terrestrial laser scanning and digital photogrammetry techniques to monitor landslide bodies. In: Orhan M (ed.) Proceedings of the XXth ISPRS congress, Istanbul, Turkey. ISPRS Archives vol. 35(B5): 246-251

Boris D (1934) Sur la sphère vide. Otdelenie Matematicheskikh i Estesvennykh Nauk 7:793–800

Brabb EE (1984) Innovative approaches to landslide hazard and risk mapping. In: 4th International Symposium on Landslides, Toronto, Canada, vol. 1: 307–323

Brabb EE (1991) The world landslide problem. Episodes 14(1):52–61

Breien H, De Blasio FV, Elverhøi A, Høeg K (2008) Erosion and morphology of a debris flow caused by a glacial lake outburst flood, Western Norway. Landslides 5:271–280

Brideau MA, Sturzenegger M, Stead D, Jaboyedoff M, Martin M, Roberts N, Ward B, Millard T, Clague J (2012) Stability analysis of the 2007 Chehalis lake landslide based on long-range terrestrial photogrammetry and airborne LiDAR data. Landslides 9:75–91

Brown ET (1981) Rock characterization testing and monitoring. Ed. Pergamon Press, Oxford

Brückl E, Brunner FK, Kraus K (2006) Kinematics of a deep-seated landslide derived from photogrammetric, GPS and geophysical data. Eng Geol 88(3-4):149–159

Carrara A (1983) A multivariate model for landslide hazard evaluation. Math Geol 15:403–426

Carrara A, Cardinali M, Detti R, Guzzetti F, Pasqui V, Reichenbach P (1991) GIS techniques and statistical models in evaluating landslide hazard. Earth Surf Process Landf 16(5):427–445. doi:10.1002/esp.3290160505

Carrara A, Cardinali M, Guzzetti F, Reichenbach P (1995) GIS technology in mapping landslide hazard. In: Carrara A, Guzzetti F (eds) Geographical Information Systems in assessing natural hazards. Kluwer Academic Publisher, Dordrecht, pp p135–p175

Carrara A, Crosta GB, Frattini P (2003) Geomorphological and historical data in assessing landslide hazard. Earth Surf Process Landf 28(10):1125–1142

Casson B, Delacourt C, Baratoux D, Allemand P (2003) Seventeen years of the "La Clapière" landslide evolution analysed from ortho-rectified aerial photographs. Eng Geol 68(1-2):123–139

Chacón J, Irigaray C, Fernández T (1993) Methodology for large scale landslide hazard mapping in a G.I.S. Seventh International Conference & Field Workshop on Landslides. pp. 77-82. Bratislava, Slovakia, Septiembre 1993. In "Landslides" Ed. Balkema. ISBN: 90-5410-302-7

Chacón J, Irigaray C, El Hamdouni R, Fernández T (1996) From the inventory to the risk analysis: improvements to a large scale G.I.S. method. In: Chacón J, Irigaray C, Fernández T (eds) Landslides. Balkema, Rotterdam. 8th ICFL Granada, Spain, p335-342

Chacón J, Irigaray C, Fernández T, El Hamdouni R (2006) Engineering geology maps: landslides and Geographical Information Systems (GIS). Bull Eng Geol Environ 65:341–411. doi:10.1007/s10064-006-0064-z

Chacón J, Irigaray C, El Hamdouni R, Jiménez-Perálvarez JD (2010) Diachroneity of landslides. In: Williams AL, Pinches GM, Chin CY, McMorran TJ, Massey CI (eds) Geologically active, vol. 1. CRC Press/Balkema, Taylor & Francis Group, Leiden, pp 999–1006. ISBN 978-0-415-60034-7

Chandler JH, Brunsden D (1995) Steady state behaviour of the Black Ven mudslide: the application of archival analytical photogrammetry to studies of landform change. Earth Surf Process Landf 20(3):255–275

Chung CF, Frabbri AG (1999) Probabilistic prediction models for landslide hazard mapping. Photogramm Eng Remote Sens 65(12):1389–1399

Corominas J, Moya J (2008) A review of assessing landslide frequency for hazard zoning purposes. Eng Geol 102:193–213

Corominas J, Van Westen JC, Frattini P, Cascini L, Malet JP, Fotopoulou S, Catani F, Van Den Eeckhaut M, Mavrouli O, Agliardi F, Pitilakis K, Winter MG, Pastor M, Ferlisi S, Tofani V, Hervás J, Smith JT (2013) Recommendations for the quantitative analysis of landslide risk. Bull Eng Geol Environ 73(2):209–263. doi:10.1007/s10064-013-0538-8

Crosta GB, Frattini P (2008) Rainfall-induced landslides and debris flows. Hydrol Process 22(4):473–477. doi:10.1002/hyp.6885

Cruden DM, Varnes DJ (1996) Landslides types and processes. In: Turner AK, Schuster RL (eds) Landslides: investigation and mitigation. National Academic Press, Washington, DC, pp 35–76, **Sp-Rep 247**

Delacourt C, Allemand P, Berthier E, Raucoules D, Casson B, Grandjean P, Pambrun C, Varel E (2007) Remote-sensing techniques for analysing landslide kinematics: a review. Bull Soc Geol Fr 178(2):89–100

Dikau R, Schrott L (1999) The temporal stability and activity of landslide in Europe with respect to climatic change (TESLEC): main objectives and results. Geomorphology 30:1–12

Dunning SA, Rosser NJ, Massey CI (2010) The integration of terrestrial laser scanning and numerical modelling in landslide investigations. Q J Eng Geol Hydrogeol 43:233–247

El Hamdouni R, Irigaray C, Fernández T, Sanz de Galdeano C, Chacón J (2003) Susceptibilidad a los movimientos de ladera en borde S.O. de Sierra Nevada (España): Implicación de la tectónica activa como factor determinante. In: Ayala-Carcedo FJ, Corominas J (eds) Mapas de susceptibilidad a los movimientos de ladera con técnicas SIG. Fundamentos y Aplicaciones en España. I.G.M.E, Madrid, pp p155–p168

Fell R, Corominas J, Bonnard C, Cascini L, Leroi E, Savage WZ (2008) Guidelines for landslide susceptibility, hazard and risk zoning for land-use planning. Eng Geol 102(3-4):85–98. doi:10.1016/j.enggeo.2008.03.022

Fernández T, Irigaray C, El Hamdouni R, Chacón J (2003) Methodology for landslide susceptibility mapping by means of a GIS. Application to the Contraviesa Area (Granada, Spain). Nat Hazards 30(3):297–308

Fernández T, Pérez JL, Cardenal J, Delgado J, Irigaray C, Chacón J (2011) Evolution of a diachronic landslide by comparison between different DEMs obtained from Digital Photogrammetry Techniques in Las Alpujarras (Granada, Southern Spain). In: Conference of Geoinformation for Disaster Management (GI4DM). Antalya, Turquía, 6pp

Flageollet JC (1996) The time dimension in the study of mass movements. Geomorphology 15(3-4):185–190

Gentili G, Giusti E, Pizzaferri G (2002) Photogrammetric techniques for the investigation of the Corniglio landslide. In: Allison RJ (ed) Applied geomorphology. Wiley, Chichester, pp p39–p48

Giussani A, Scaioni M. (2004) Application of TLS to support landslides study: survey planning, operational issues and data processing. ISPRS Archives 36(8/W2): 318-323

Glenn NF, Streutker DR, Chadwick DJ, Thackray GD, Dorsch SJ (2006) Analysis of LiDAR-derived topographic information for characterizing and differentiating landslide morphology and activity. Geomorphology 73:131–148

Gómez-Pugnaire MT, Galindo-Zaldívar J, Rubatto D, González-Lodeiro F, López V, Jabaloy A (2004) A reinterpretation of the Nevado-Filábride and Alpujárride complexes (Betic Cordillera): field, petrography and U-Pb ages from orthogneisses (western Sierra Nevada, S Spain). Schweiz Miner Petrogr Mitt 84(3):303–322

González-Díez A, Fernández-Maroto G, Doughty MW, Díaz de Terán JR, Bruschi V, Cardenal J, Pérez JL, Mata E, Delgado J (2014) Development of a methodological approach for the accurate measurement of slope changes due to landslides, using digital photogrammetry. Landslides 11(4):615–628. doi:10.1007/s10346-013-0413-5

Guzzetti F (2002) Landslide hazard assessment and risk evaluation: overview, limits and prospective. Proceedings 3rd MITCH Workshop Floods, Droughts and Landslides, p24-26

Guzzetti F, Carrara A, Cardinali M, Reichenbach P (1999) Landslide hazard evaluation: a review of current techniques and their application in a multi-scale study, Central Italy. Geomorphology 31(1-4):181–216. doi:10.1016/S0169-55X(99)00078-1

Guzzetti F, Reichenbach P, Cardinali M, Galli M, Ardizzone F (2005) Probabilistic landslide hazard assessment at the basin scale. Geomorphology 72(1-4):272–299. doi:10.1016/j.geomorph.2005.06.002

Guzzetti F, Mondini AC, Cardinali M, Fiorucci F, Santangelo M, Chang KT (2012) Landslide inventory maps: new tools for an old problem. Earth Sci Rev 112(1):42–66. doi:10.1016/j.earscirev.2012.02.001

Hoek E, Brown ET (1980) Empirical strength criterion for rock masses. J Geotech Engng Div, ASCE 106 (GT9): 1013-1035

Hoek E, Brown E (1997) Practical estimates of rock mass strength. Int J Rock Mech Min Sci 34:1165–1186

Hunt RE (2005) Geotechnical engineering investigation manual, 2nd edn. CRC Press, Taylor & Francis Group, Leiden, 256pp. ISBN 978-0-8493-2182-5

IGN (2008-2012) Plan Nacional de Ortofotografía Aérea (National Plan of aerial orthophotography). Instituto Geográfico Nacional de España (National Geographic Institute of Spain). http://www.ign.es/PNOA/presentacion.html. Accessed 22 Jan 2015

Irigaray C, Palenzuela JA (2013) Análisis de la actividad de movimientos de ladera mediante láser escáner terrestre en el suroeste de la Cordillera Bética (España). Revista de Geología Aplicada a la Ingeniería y al Ambiente 31:53–67

Irigaray C, Chacón J, Fernández T, (1996) Comparative analysis of methods for landslide susceptibility mapping. In: Chacón J, Irigaray C, Fernández T (eds) Landslides. Balkema, Rotterdam. 8th ICFL Granada, Spain, p373-384

Irigaray C, Lamas F, El Hamdouni R, Fernández T, Chacón J (2000) The importance of the precipitation and the susceptibility of the slopes for the triggering of landslides along the roads. Nat Hazards 21(1):65–81. doi:10.1023/A:1008126113789

Irigaray C, Fernández T, El Hamdouni R, Chacón J (2007) Evaluation and validation of landslide-susceptibility maps obtained by a GIS matrix method: examples from the Betic Cordillera (southern Spain). Nat Hazards 41(1):61–79. doi:10.1007/s11069-006-9027-8

ISRM (International Society for Rock Mechanics) (1978) Suggested methods for determining hardness and abrasiveness of rocks. Int J Rock Mech 15:89–97

Iverson RM (2000) Landslide triggering by rain infiltration. Water Resour Res 36(7):1897–1910. doi:10.1029/2000wr900090

Jiménez-Perálvarez JD (2012) Movimientos de ladera en la vertiente meridional de Sierra Nevada (Granada, España): identificación, análisis y cartografía de susceptibilidad y peligrosidad mediante SIG. PhD Thesis, Department of Civil Engineering University of Granada, Spain, 188pp

Jiménez-Perálvarez JD, Irigaray C, El Hamdouni R, Chacón J (2011) Landslide-susceptibility mapping in a semi-arid mountain environment: an example from the southern slopes of Sierra Nevada (Granada, Spain). Bull Eng Geol Environ 70:265–277. doi:10.1007/s10064-010-0332-9

Lichti DD, Jamtsho S (2006) Angular resolution of terrestrial laser scanners. Photogrammetric Rec 21:141–160

Lichti DD, Gordon SJ, Stewart MP (2002) Ground-based laser scanners: operation, systems and applications. Geomatica 56:21–33

Mayne PW, Christopher BR, DeJong J (2001) Manual on Subsurface Investigations, FHWA NHI-01-031. National Highway Institute and FHWA. U.S. DOT, Washington DC

Monserrat O, Crosetto M (2008) Deformation measurement using terrestrial laser scanning data and least squares 3D surface matching. ISPRS J Photogramm Remote Sens 63(1):142–154. doi:10.1016/j.isprsjprs.2007.07.008

Oppikofer T, Jaboyedoff M, Blikra L, Derron MH, Metzger R (2009) Characterization and monitoring of the Åknes rockslide using terrestrial laser scanning. Nat Hazards Earth Syst Sci 9:1003–1019

P/WLI (1995) A suggested method for describing the rate of movement of a landslide. International Geotechnical Societies' UNESCO Working Party on World Landslide Inventory; Chairman Bonnard CH. Bull Eng Geol Environ 52:75–78

Palenzuela JA, Irigaray C, Jiménez-Perálvarez JD, Chacón J (2013) Application of terrestrial laser scanner to the assessment of the evolution of diachronic landslides. In: Margottini C, Canuti P, Sassa K (eds) Landslide science and practice, vol 2. Springer, Berlin, pp 517–523. ISBN 978-3-642-31445-2

Palenzuela JA, Marsella M, Nardinocchi C, Pérez JL, Fernández T, Chacón J, Irigaray C (2014) Landslide detection and inventory by integrating LiDAR data in a GIS environment. Landslides, Online First October 2014, 16pp. doi: 10.1007/s10346-014-0534-5

REDIAM (Environmental Information Network of Andalusia) (2014) Service for download ortofotographs and data from the territory. Council of Andalucía. URL: http://www.juntadeandalucia.es/medioambiente/site/rediam/menuitem.aedc2250f6db83cf8ca78ca731525ea0/?vgnextoid=0863d61d8470f210VgnVCM2000000624e50aRCRD&lr=lang_en. Accessed 22 Jan 2015

Riegl (2010) Terrestrial scanning, http://www.riegl.com/products/terrestrial-scanning/, Riegl Laser Measurement Systems GmbH. Horm, Austria

Rodríguez-Peces MJ, García-Mayordomo J, Azañón JM (2009) Evaluación regional de inestabilidades de ladera inducidas por terremotos para diferentes escenarios sísmicos en Sierra Nevada (Granada, SE España). In: Alonso E, Corominas J, Hürlimann M (eds) VII Simposio Nacional sobre Taludes y Laderas Inestables, Barcelona, vol. 2: 687–698

Rosser NJ, Petley DN, Lim M, Dunning SA, Allison RJ (2005) Terrestrial laser scanning for monitoring the process of hard rock coastal cliff erosion. Q J Eng Geol Hydrogeol 38:363–375

Scaioni M (2005) Direct georeferencing of TLS in surveying of complex sites. Int Arch Photogram Rem Sens Spatial Inform Sci 36:8

Schmertmann JH (1975) Measurement of in-situ shear strength. Proc ASCE Specialty Conf. on In situ measurement of soil properties, Raleigh vol. 2

Soeters R, Van Westen JC (1996) Slope instability recognition, analysis, and zonation. In: Turner AK, Schuster RL (eds) Landslides: investigation and mitigation. National Academic Press, Washington, DC, Sp-Rep 247, p129-177

Sterzai P, Vellico M, Berti M, Coren F, Corsini A, Rosi A, Mora P, Zambonelli F, Ronchetti F (2010) LiDAR and hyperspectral data integration for landslide monitoring. Int J Remote Sens 42(3):89–99

Teza G, Galgaro A, Zaltron N, Genevois R (2007) Terrestrial laser scanner to detect landslide displacement fields: a new approach. Int J Remote Sens 28:3425–3446

Thornes JB, Alcántara-Ayala I (1998) Modelling mass failure in a Mediterranean mountain environment: climatic, geological, topographical and erosional controls. Geomorphology 24(1):87–100

Van Westen CJ, Van Asch TW, Soeters R (2006) Landslide hazard and risk zonation—why is it still so difficult? Bull Eng Geol Environ 65(2):167–184. doi:10.1007/s10064-005-0023-0

Varnes DJ (1984) Landslide hazard zonation: a review of principles and practice. Commission on Landslides of the IAEG, UNESCO, Paris. Natural Hazards Series 3, 63pp

Walstra DJR, van Rijn LC, Klein A (2004) Validation of a new transport formula (TRANSPOR2004) in a three-dimensional morphological model. In: Smith JM (ed.) Proc. 29th Int. Conf. on Coastal Engineering, Lisbon, Portugal, p. 2703-2715

Walstra J, Chandler JH, Dixon N, Dijkstra TA (2007) Aerial photography and digital photogrammetry for landslide monitoring. In: Teeuw RM (ed) Mapping hazardous terrain using remote sensing, vol 283, Geological Society, London, Special Publications., pp p53–p63

Wieczoreck GF (1996) Landslide triggering mechanisms. In: Turner AK, Schuster RL (eds) Landslides investigation and mitigation, vol 247, Special Report. TRB National Research Council. National Academy Press, Washington, DC, pp 76–90

WP/WLI (1993) A suggested method for describing the activity of a landslide. International Geotechnical Societies' UNESCO Working Party on World Landslide Inventory; Chairman Cruden DM. Bull Eng Geol Environ 47:53–57

Zhang W, Chen Y, Zhan L (2006) Loading/Unloading response ratio theory applied in predicting deep-seated landslides triggering. Eng Geol 82(4):234–240. doi:10.1016/j.enggeo.2005.11.005

J. A. Palenzuela · J. D. Jiménez-Perálvarez (✉) · R. El Hamdouni ·
P. Alameda-Hernández · J. Chacón · C. Irigaray
Department of Civil Engineering,
ETSICCP, University of Granada, Spain,
Campus Fuentenueva s/n, Granada, 18071, Spain
e-mail: jorgejp@ugr.es